Enhancing Leak Location in Buried Water Pipes using Array Signal Processing Techniques: the Effect of Wave Velocity Variation

Journal of Physics: Conference Series **2647** (2024) 082011 doi:10.1088/1742-6596/2647/8/082011

Enhancing Leak Location in Buried Water Pipes using Array Signal Processing Techniques: the Effect of Wave Velocity Variation

P H Matos[1], J M Muggleton[2], M J Brennan[2,3], F C L Almeida[3], B C Campos[3], P J Paupitz[3], M K Iwanaga[3], M Karimi[4], E Rustighi[1]

[1]Department of Industrial Engineering, University of Trento, Povo, Italy
[2]University of Southampton, Institute of Sound and Vibration Research Highfield campus, Southampton, UK
[3]Department of Mechanical Engineering, UNESP, Bauru, Sao Paulo, Brazil
[4]School of Mechanical and Manufacturing Engineering, University of New South Wales, Sydney, Australia

Corresponding author: ph.demelocasadomatos@unitn.it

Abstract. Leakage in buried pipelines is a significant cause of water wastage in distribution systems, resulting in water losses ranging from 30% to 50% in many countries. To address this issue, techniques have been developed to detect leaks in buried pipes over the last few decades. The leak detection procedure typically involves three steps: (1) leak detection, which involves analysis of water pressure/flow measurements along the pipelines; (2) estimation of the approximate region where the leak occurred through local pressure variations; and (3) pinpointing the estimated location of the leak to perform maintenance procedures. Acoustic pinpointing techniques are among the most effective ones to deal with the latter step. These techniques exploit the delays in time of arrival of acoustic waves, caused by the leak, between different sensors placed around the suspected leak. By calculating the cross-spectral densities (CSDs) between sensors and analysing their phase difference over frequency, it is possible to infer the estimated location of the radiating source. Existing methods rely on access points to the pipeline through correlators. However, the buried pipe acts as a radiating source, and its location could also be estimated through ground vibration signals. Although array signal processing techniques applied to source localization are well-established in the acoustics field, their adaptation to the vibroacoustic field is less well developed. Among the many challenges, the identification of wave velocity is one of the most troublesome. In this paper, the effect of the wave velocity variation on the leak pinpointing is investigated and tested against numerical data. Results show that the estimation of the leak position is sensitive to the wave velocity variabilities. The pinpointing error is found to be more significant in terms of the depth of the pipe, compared to the error on the ground surface.

1. Introduction

Leakage in buried pipelines is a significant cause of water wastage in distribution systems, resulting in water losses ranging from 30% to 50% in many countries [1,2]. Efforts to reduce water loss in water distribution systems have resulted in the proposal and investigation of several techniques over the past

few decades. Of these techniques, cross correlation and vibroacoustic methods have emerged as the most prominent.

Cross-correlation techniques estimate the leak position from the time delays between the arrival of leak noise at the sensors, which are placed directly into the pipe or in access points such as hydrants at knowing positions. These techniques have been investigated in depth, for example by [3-5] and are well established, especially for metallic pipes. The technique performs well for a range of situations; however, it is limited by high wave attenuation in polymeric pipes, which are widely used in water distribution systems nowadays, and by the estimation of the leak noise velocity, which is also highly dependent on the pipe material and geometry, and the surround medium (soil properties) [11,12].

In the context of acoustics, many techniques to identify acoustic sources and estimate their power have been well developed and formalized [9]. The general picture consists of an array of microphones measuring the pressure field caused by an acoustic source, and by applying spatiotemporal filters to the pressure signals, the locations radiating most acoustic energy and their amplitudes may be mapped. This field is named acoustic imaging and relies on array signal processing techniques. In the context of source estimation, the former is widely known as beamforming, and it is applied in many different other engineering fields such as radio antenna design and seismic wave detection [10]. The techniques are mainly limited by the number of sensors and their spatial distribution, which defines the maximum measurable frequencies and the resolution of the signal spectrum.

Recently, [11] proposed the application of acoustic imaging techniques to pinpoint a leak as a complementary approach to the existing methods. The paper investigated the effect of the measurement direction on the beamforming output, and results showed that measurements normal to the ground surface are sufficient to detect a leak from a buried pipe. However, other challenges are yet to be investigated. In acoustic imaging, the wave velocity is often well defined within a narrow range around the speed of sound in air. However, for pinpointing leaks by using sensors on the ground surface, multiple wave-types need to be accounted for that propagate through the ground with different velocities and amplitudes.

This paper investigates the effect of the wave velocity variation on the steering vector when applying the beamforming technique to leak pinpointing estimation in buried pipes. From the beamforming formulation, it is possible to obtain an expression that relates the beamforming output maximum position with the steering vector wave velocity. Numerical data are used as inputs for a conventional beamforming (CB) formulation to locate a simulated leak for different wave velocities. The paper is organized as follows. Section 2 provides a discussion about the beamforming formulation from which an expression relating beamforming output and wave velocity is derived. Section 3 presents details of the numerical simulation used to generate the data. In Section 4 the results are presented and discussed. Finally, Section 5 presents the concluding remarks and future research topics.

2. Analysing wave velocity variation on leak pinpointing with beamforming

In this section, an expression that relates the beamforming output with the wave velocity variation is derived from an analytical formulation. A general overview on the topic is provided followed by the mathematical definitions.

Array signal processing is a branch of signal processing that focuses on signals acquired from propagating waves travelling through an array of sensors. By combining the information from individual sensors in the array, it is possible to enhance the signal-to-noise ratio, track the energy radiated by moving sources, and estimate the number of sources and their locations along with their frequency content. The branch of array signal processing that deals with source estimation may be divided in two global classifications: beamforming and inverse methods. The authors in [9,10] present a complete review of the methods and compare them using numerical data. The advantages and limitations of each technique are discussed in depth as well as their constraints.

This paper explores the beamforming formulation to estimate source position. The idea is the following: an array of M sensors measure a wavefield $s(r_{sm}, \omega)$ radiated by a source in position $\mathbf{r}_s =$

(x_s, z_s) and measured at the points $\mathbf{r}_m = (x_m, z_m)$, in which z_m is set to 0 and $r_{sm} = |\mathbf{r}_s - \mathbf{r}_m|$ is the distance between source and sensors. An analytical propagation model $v(r_{pm}, k_p)$ is defined, commonly called the steering vector, and it simulates the array signal given a virtual source at position $\mathbf{r}_p$ with wavenumber k_p. Again, $r_{pm} = |\mathbf{r}_p - \mathbf{r}_m|$ is the distance between control point and sensors. Both spectra are multiplied, and the beamforming output $y(\mathbf{r}_\mathrm{p})$ is calculated for a set of arbitrary control points $\mathbf{r}_p = (x_p, z_p)$. When the control point coincides with the source position $\mathbf{r}_s$, both spectra have a similar shape, and the beamforming output reaches a maximum. This output may be represented in a map in which the coordinates are the control points, and the intensity is the beamforming output amplitude. Thus, the whole operation may be interpreted as the convolution between the measured signal and an analytical signal through a set of control points. Figure 1 presents a schematic for a planar case showing the source, the control point and their angles of arrival at a sensor in position x_m.

It follows that there are two parameters that must be pre-defined to calculate the steering vector: the control point $\mathbf{r}_p$ and a wavenumber k_p. When both the signal (k_s) and the steering vector (k_p) wavenumbers are the same, scanning through the control points should lead to the correct position of the source. However, if they differ, the control point in which the output will be a maximum will be different from the actual source position. A wideband propagating signal is defined as $s(r_{sm}, \omega) = S(\omega)\exp(-\mathrm{i}k_s r_{sm})$ with wavenumber k_s, amplitude $S(\omega)$ and relative distance to the sensors r_{ms}. The steering vector is defined as a complex exponential $v(\mathrm{r}_{pm}, k_p) = \exp(-\mathrm{i}k_p r_{pm})$ with wavenumber k_p and relative distance to the sensors r_{pm}.

The beamforming operation is described in the form of an equation as

$$y(\boldsymbol{r}_p, \omega) = S(\omega)\sum_{m=0}^{M}\exp\left(\mathrm{i}(k_p r_{pm} - k_s r_{sm})\right) \quad (1)$$

Eq. (1) can be seen as a bandpass filtering operation, in which the content of the signal spectrum is amplified around k_p and attenuated in the remainder, for fixed r_{pm} and r_{sm}. The filter has a similar shape of the sinc function and is defined by a main lobe centered in k_p surrounded by several sidelobes with decreasing amplitude. The main lobe defines the passband region with a bandwidth of ~$4\pi/L$, in which L is the length of the signal. The sidelobes defines the attenuating region. As the value of k_p changes, the filter shifts through the frequency spectrum of the signal, amplifying and attenuating different regions. When the value of k_p matches k_s, the filter output will be an amplified version of the original signal and that is reflected as a maximum peak in the beamforming output map $y(\mathbf{r}_p, \omega)$.

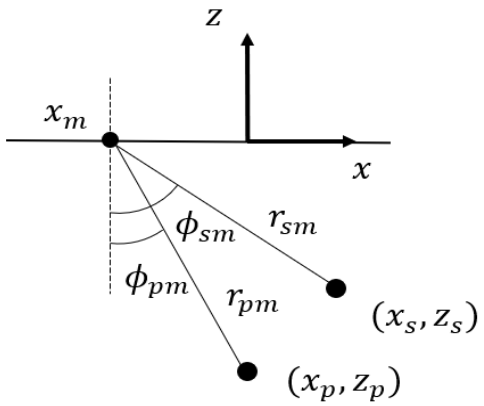

Figure 1. 2D schematic with the source at position (x_s, z_s), the control point at (x_p, z_p), the sensor location (x_m, z_m) and the angles of arrival ϕ_{pm} and ϕ_{sm}. The distances between source/control point and sensors are r_{sm} and r_{pm}.

Now, to verify how the wavenumber difference is reflected in the source mapping, it should be noted that the wavenumber measured by the array is the trace wavenumber of the propagating wave over the array, and the trace wavenumber depends on the angle between the source and the m-th sensor, $\phi_{sm} = \text{atan}\frac{(x_m - x_s)}{z_s}$, as shown in figure 1. For this reason, the wavenumber spectrum contains different components of the source wavenumber k_s multiplied by $\sin(\phi_{sm})$. The same is true for the steering vector wavenumber spectrum. Thus, it is possible to estimate the angles of arrival between the peak location in the map and each sensor through the expression $\phi_{pm} = \text{asin}\left(k_s/k_p \sin\phi_{sm}\right)$. Since $\tan\phi_{pm} = (x_p - x_m)/z_p$, it is possible to obtain the peak coordinates, $x_{p_{\text{peak}}}$ and $z_{p_{\text{peak}}}$ by writing the problem as a linear system of M equations and two variables

$$\begin{bmatrix} 1 & -\tan\phi_{p0} \\ \vdots & \vdots \\ 1 & -\tan\phi_{pM} \end{bmatrix} \begin{bmatrix} x_{p_{\text{peak}}} \\ z_{p_{\text{peak}}} \end{bmatrix} = \begin{bmatrix} x_0 \tan\phi_{p0} \\ \vdots \\ x_m \tan\phi_{pm} \end{bmatrix}. \tag{2}$$

which can be written as **Ax**=**b**. To solve the equations, a pre-multiplication by the transpose of **A** is performed to obtain a 2 by 2 square matrix followed by another pre-multiplication by the pseudoinverse, resulting in $\mathbf{x} = \left(\mathbf{A^T A}\right)^{-1}\left(\mathbf{A^T b}\right)$. The solutions for $x_{p,\text{peak}}$ and $z_{p,\text{peak}}$ are obtained as

$$\begin{aligned} x_{p,\text{peak}} &= \frac{-A_1}{(A_1^2 - MA_2)} \sum_{m=0}^{M} x_m \tan\left(\phi_{pm}\right) \\ z_{p,\text{peak}} &= \frac{M}{(A_1^2 - MA_2)} \sum_{m=0}^{M} x_m \tan\left(\phi_{pm}\right) \end{aligned} \tag{3}$$

where $A_1 = \sum_{m=0}^{M} \tan\left(\phi_{pm}\right)$ and $A_2 = \sum_{m=0}^{M} \tan^2\left(\phi_{pm}\right)$.

Two preliminary conclusions can be drawn by analysing Eqs. (3). First, when the horizontal position of the source coincides with the middle of the array, the angles of arrival for the sensors on the left side will oppose those of the right, so that $A_1 = 0$. Thus, for this case only the depth will be affected by the wavenumber difference.

Second, the position deviations are dependent on the wavenumber ratio implicitly as a function of $\phi_{pm} = \text{asin}\left(k_s/k_p \sin\phi_{sm}\right)$. Note that, for values in which $k_p < k_s$, the argument of the arcsine function may become greater than one for sensors horizontally away from the source. This condition limits the applicability of the expression with increasing k_s/k_p because it causes the angles of arrival to become complex. The arcsine output for numbers greater than one have a constant real part equal to $\pi/2$ and an imaginary part proportional to the logarithm of the number. The real part of the tangent of a complex number with a real part equal to $\pi/2$ tends to zero. In fact, the behavior of both curves with changes in k_s/k_p is that, as k_p tends to zero, more terms in the sum become complex and the real part of more terms tends to zero. In contrast, as k_p approaches infinity, $\tan(\phi_m) \to 0$ and y_p tends to infinity due to the A_2 term in the denominator reaching zero faster than the sum in the numerator.

For the case in which $k_p \sim k_s$, the output will be in the vicinity of the source, and the position deviation with k_p is proportional to the actual source depth y_s and the signal length L. It is possible to derive another expression to estimate the wavenumber ratio in which the angles of the sensors further from the source start to become complex. This happens when $\sin\phi_{p0} = 1$, then it is possible to obtain the wavenumber ratio in which Eq. (2) tends to zero by substituting $k_s/k_{p,\text{peak}} = 1/\sin\phi_{s0}$. From this point, as $k_s/k_{p,\text{peak}}$ increases, the output position rapidly approaches zero.

Figure 2 shows the curves for $x_{p,\text{peak}}/x_s$ and $z_{p,\text{peak}}/z_s$ as a function of k_s/k_p for a uniform linear array with 3 sensors spaced 0.5 meters apart. The position of the source is $x_s = z_s = 1$ meter.

Only the real part of the peak coordinates is plotted. The threshold at which $x_{p,\text{peak}}$ and $z_{p,\text{peak}}$ rapidly approaches zero is represented as a vertical black line. From the figure it becomes clear that the variations in position along $z_{p,\text{peak}}$ are more sensitive than the ones along $x_{p,\text{peak}}$. Moreover, the output position may rapidly decay to zero even for a small variation on the wavenumber of the steering vector depending on the position of the threshold adopted. In figure 2, an increase of only 20% of the wavenumber ratio outputs the peak at the origin. It also becomes clear that, for this case, $z_{p,\text{peak}}$ almost doubles for k_s/k_p~0.8, whereas $x_{p,\text{peak}}$ roughly increases 20%.

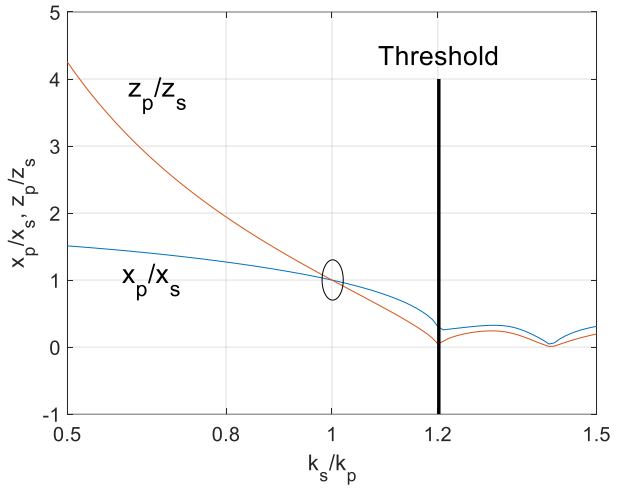

Figure 2. The ratio between the maximum output coordinates, x_p and z_p, and the actual source position x_s, z_s. After k_s/k_p reaches the threshold, the angles of arrival start to become complex and the peak position tends to the origin.

This section provided an analysis of the steering vector wavenumber variation on the peak position of the output map. From the considered model, a linear system of equations was solved, and an expression of the peak position was obtained as a function of the angles of arrival between the source and sensors ϕ_{sm}, and the number of sensors M and the wavenumber ratio k_s/k_p. The expression predicts that the peak position is more biased along the depth (z direction) than on the surface (x direction). This means that an underestimation of the wavenumber as an initial guess could be a good approach to deal with the wavenumber discrepancy. In the results section, which will be introduced later in the text, it is shown that this is also observed in the numerical data.

3. Wave propagation model

This section provides a brief description of the wave-types involved in leak position estimation and the importance of developing numerical simulation under controlled conditions. Hence, the main aspects of the simulation and the predicted dispersion curves are presented herein in this section.

Analytical models to describe the dynamics of buried pipelines have been developed since last century [12]. From the beginning of the past decade, further studies on the response of buried fluid-filled pipes due to leak type excitation have been carried out to develop analytical expressions to predict the fluid-borne wavenumber, as an auxiliary tool to the correlation techniques [17]. It was established that the axisymmetric fluid-borne wave is excited by pressure waves in the fluid within the pipe, and it is the main carrier of leak noise energy along the pipe, which wave speed is highly affected by the shear modulus of the soil [11]. Moreover, the fluid-borne wave might radiate energy into the surrounding medium given that the wavenumber of the body waves in the medium are higher than the fluid-borne wavenumber. When that happens, shear and longitudinal waves are radiated into the soil by the pipe and these waves are measured by the array of sensors. Gao *et al* [17] developed an analytical expression

relating pipe pressure with ground displacements due to radiated shear and longitudinal waves by the pipe.

In summary, for the proposed application, the shear and longitudinal waves radiated by the leak-pipe system are of great importance. Their propagation velocity depends on the soil mass and elastic properties. The velocity ratio between both waves is bounded by the Poisson's constant of the medium, and the longitudinal wave always propagates at higher wave speed. The simulation was set using the properties of the Blithfield experimental rig in UK [3] and are summarised in Table 1.

Table 1. Pipe and soil properties considered in the simulation.

Pipe Properties	
Young's Modulus (N/m^2)	2 x 10^9
Density ρ_p (kg/m^3)	900
Mean Radius (mm)	84.5
Wall Thickness (mm)	11
Loss factor η_p	0.06

Soil Properties	
Bulk modulus (N/m^2)	5.3 x 10^7
Shear modulus (N/m^2)	2.0 x 10^7
Density (kg/m^3)	2000
Bulk and shear loss factors	0.15

The water-pipe-soil system was analysed using a 2D axisymmetric finite element model developed in COMSOL Multiphysics software (v5.2). The simulation was conducted in the frequency domain with a frequency range of 50 to 500 Hz in steps of 10 Hz. A monopole source was placed at the centre of a 20-meter-long cylindrical shell filled with water to simulate a leak in the pipe. The computational domain was discretised using rectangular quadratic (second order) Lagrange elements, and a fine mesh was used to ensure accurate numerical predictions. A Perfectly Matched Layer (PML) element was applied to the boundary of the computational domain to minimise reflections of outgoing waves. The pipe wall and surrounding fluid was meshed with element size of 3 mm, while the soil further away from the pipe was discretised with element size of 30 mm. The water was modelled as a fluid using the COMSOL Pressure Acoustics module, while the pipe and soil were modelled as linear elastic media using the Solid Mechanics module. The Acoustic-Structure boundary condition was used to couple the pressure acoustics model to the structural component. The simulation was performed with the monopole source placed at the origin of the domain, and the frequency domain was used for numerical computations to obtain the response of the water-pipe-soil system under monopole source excitation. The simulation output is the mobility of soil particles in a plane grid of 5 by 5 points at coordinates $(x_m, y_m, 1)$ distant 0.5 meters apart, comprising an area of 2 by 2 meters. The plane where the mobilities were taken is one meter distant from the centre of the pipe. This grid was chosen to have the first sensor of the array vertically aligned with the monopole. Figure 3 shows a simplified description of the simulation with the coordinate system. The particle velocities are taken in three directions w, v and u, but only w was considered for this paper. The numerical data is used as input for the conventional beamforming (CB) formulation to estimate the monopole location (i.e., leak source)

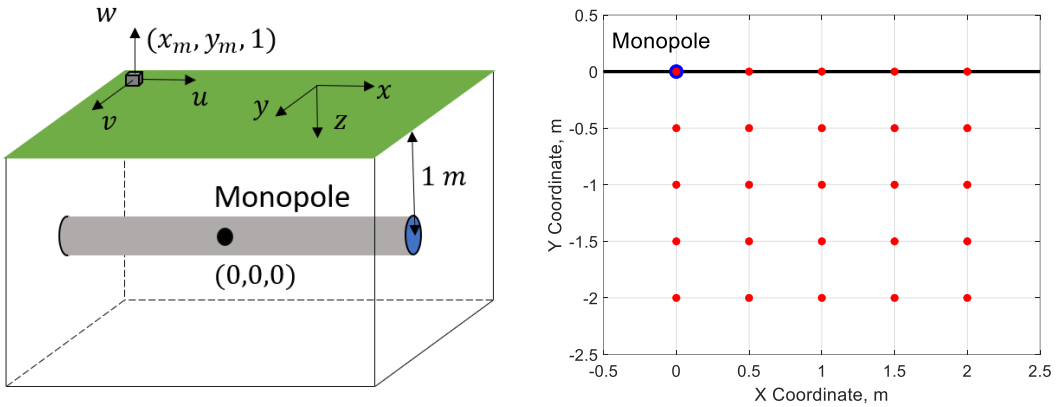

Figure 3. Schematic of the simulation (left) and upper view of the array (right). The monopole is inside the pipe and the measurement plane is one meter above. The particle velocities are taken over a grid of 5 by 5 points at positions (x_m, y_m) represented as the red dots on the left. The first sensor of the array is vertically aligned with the monopole.

The non-dimensional dispersion curves of each propagating wave in the simulation are plotted in figure 4. The wavenumber is multiplied by the sensors spacing $d = 0.5$ meters, and the aliasing limit for which the array may detect the waves is π. The limit is added to the figure as a reference for convenience. The figure shows that the array can only operate in a considerable frequency range without suffering aliasing, given that the longitudinal wave dominates the system response, which is observed in the vicinity of the monopole source.

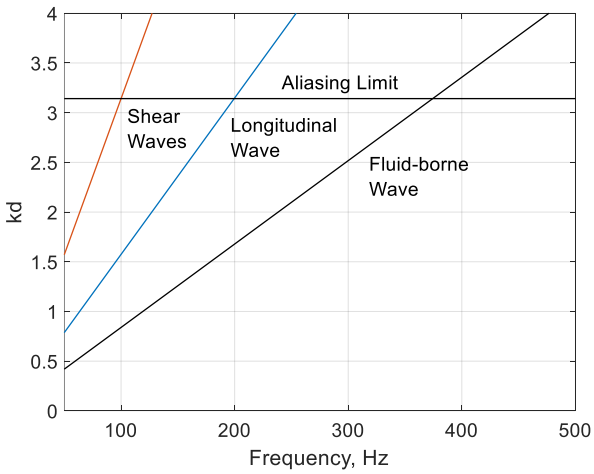

Figure 4. The non-dimensional wavenumber for the propagating waves in the simulation. The aliasing limit is added as a reference.

In summary, this section described the numerical simulation setup and presented the dispersion curves of the propagating waves in the pipe-soil system. Simulated data from a large array is available to test the beamforming technique and to assess the effect of the steering vector wavenumber variability on the results.

4. Results and Discussion

From the numerical data, an analysis to investigate the bias in the steering vector wavenumber on the position of the beamforming output peak is carried out. Besides, a performance parameter is defined as the relative distance between the actual source and the position of the output peak. Since, it was observed in Section 2 that the changes in k_p affect mostly the depth of the output, the relative distance is separated

into horizontal distance (along x and y) and vertical distance (along z). The parameters are defined simply as

$$\Delta H = \left|\mathbf{r}_s - \mathbf{r}_p\right| \qquad \Delta Z = \left|z_s - z_p\right|, \tag{4}$$

where $\mathbf{r}_{s,p} = \left(x_{s,p}^2 + y_{s,p}^2\right)^{\frac{1}{2}}$. The parameters are calculated for different values of k_p ranging from 0.5 to 1.5 the value of k_s. All cases use the same square array geometry with 5 by 5 sensors distant 0.5 meters apart. The array centre is positioned at 1 meter from the source and from the pipe, and the beamforming output is calculated over a control point region forming a cube of dimensions 5 by 5 by 5 meters beneath the array. To compare the output peak position in different directions, the map is averaged along one fixed direction, i.e., to compare the position deviation along the ground surface the map is averaged along the 5 meters in z direction. Figure 5 shows the relative distances for different values of k_s/k_p. The relative distance predicted by Eq. (3) is added as black bars, considering a 1D array with 5 sensors and same sensor spacing. The results presented in figure 5 shows that even if the wavenumber of the steering vector is half of actual one, the beamforming output still estimates the horizontal position with a deviation of only 0.25~0.5 meters from the source position but estimates the vertical position with a deviation of 2 meters. Another interesting observation is the asymmetry in relation to $k_s/k_p = 1$ for both coordinates. Above this value, ΔH drastically increases whereas ΔZ remains around unity. This is because the vertical estimate tends to zero, which is reflected in a ΔZ~1. For ΔH, the increase in deviation after $\frac{k_s}{k_p} = 1$ might be due to the fact that the averaged output is being considered to extract the peak location, thus sidelobes might contribute to the peak location in the horizontal plane in such a way that the deviation increases.

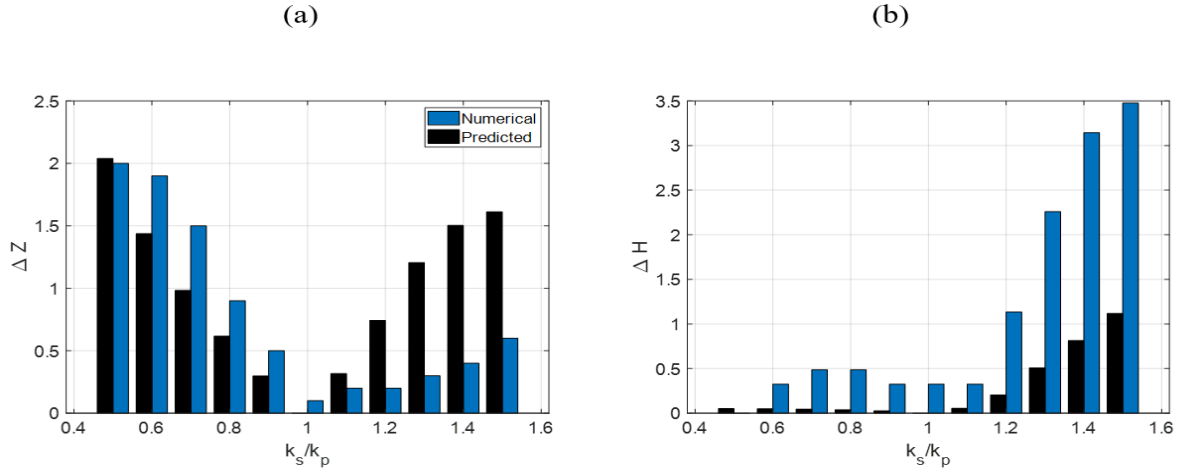

.

Figure 5. The relative distance between source and maximum output for different values of k_s/k_p. The distance along the depth (a) is more sensitive than the one along the ground surface (b). The deviation predicted from Eq. (3) is added as the black bars for comparison.

In figure 6, the red dots represent the sensors positions, the blue dot represents the monopole position and the black line is the pipe. The averaged beamforming output is shown in the colour bar next to the map. Figures 6(a)i and 6(a)ii represent the beamforming output for $k_s/k_p = 1$ and Figures 6(b)i and 6(b)ii for $k_s/k_p = 0.8$. Moreover, the captions (i) and (ii) stand for ground surface and ground depth,

respectively. It is possible to highlight that the position along the z direction deviates considerably more than the position in the xy plane, as predicted by Eq. (3).

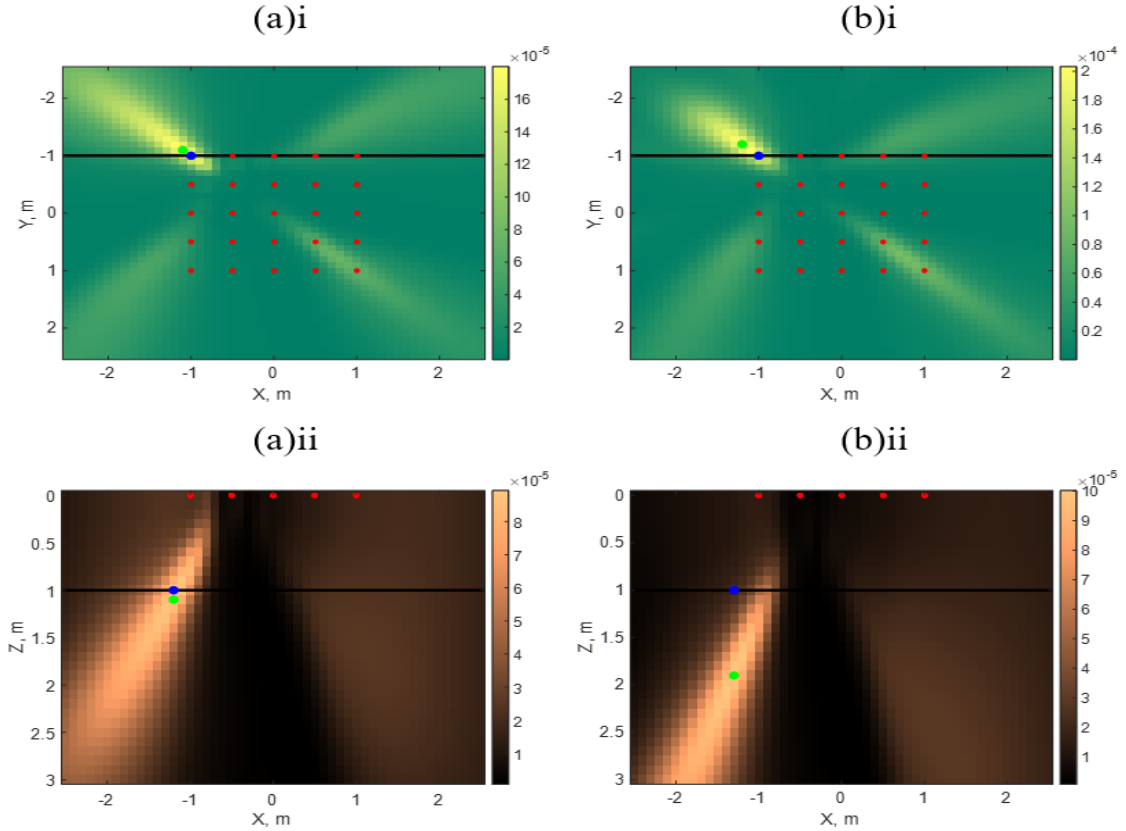

Figure 6. Beamforming output map for $k_s/k_p = 1$ (left) and $k_s/k_p = 0.8$ (right). The upper row are the maps on the xy plane (horizontal direction) and the bottom row on the zx plane (vertical direction). The red dots represent the sensors of the array, the blue dot the monopole source, the green dot the peak position and the black line the pipeline.

In summary, the beamforming output applied to the numerical data for different values of k_s/k_p were analysed to investigate the effect of k_p variation on the maximum output position. From the analytical expression it was predicted that the depth of the maximum output is more sensitive to variations of k_p than the bias on the ground surface for the leak position estimation, and this was also confirmed by the numerical data.

5. Conclusions

This paper investigated the effect of the steering vector wavenumber bias on the beamforming output for leak position estimation. From the beamforming formulation, two expressions that gives the coordinates of the beamforming output peak location were obtained and showed that the deviations in the output position along the depth are way more significant than the ones along the ground surface.

A leak-pipe system was simulated using COMSOL, and the generated data were used as input to the beamforming technique. The steering vector wavenumber was "tunned" from 0.5 to 1.5 times the value of the source wavenumber k_s and the beamforming output calculated for each value. The deviations between the actual source position (i.e., leak) and the beamforming output peak position were calculated for two different directions: one for the ground surface ΔH and the other one for the depth ΔV. The Results are in accordance with the expressions obtained in Section 2, so that the biased wavenumber of

the steering vector presents a higher impact on the depth estimation of the leak position than its location on the ground surface. Furthermore, this result contributes to the further development of a seismic camera to estimate the leak position via the beamforming technique. The results show that, even though there might be variabilities of the wavenumber, it is still possible to locate the leak with relatively good accuracy, since for most of cases the depth of the pipe is usually known, and the main challenge is to obtain the leak position along the ground surface. It is also shown that, in general, an underestimation of the wavenumber leads to a better initial estimate.

In conclusion, the beamforming performance is highly sensitive to the steering vector wavenumber, although mostly to estimate the source depth. The source position along the ground surface deviates considerably less. This result provides a useful insight into the limitations of applying array signal processing techniques to leak position estimation and broadens the way to developing more sophisticated and adapted algorithms specific for ground vibration and optimized to leak location in buried water pipes.

Acknowledgements

This project has received funding from the European Union's Horizon 2020 research and innovation programme under Grant Agreement \#101016888. The authors would also like to thank the financial support provided by the São Paulo Research Foundation (FAPESP) under the Grant numbers 2020/12251-1 and 2022/12464-0.This result only reflects the author's view and the EU is not responsible for any use that may be made of the information it contains.

References

[1] https://blogs.worldbank.org/water/what-non-revenue-water-how-can-we-reduce-it-better-water-service , last accessed: 21/03/2023
[2] A.P. Ribeiro. “O Século da Escassez”. O Globo (Printed Issue 24/03/2018, p.8).
[3] F.C.L. Almeida, M.J. Brennan, P.F. Joseph, S. Dray, P.F. Whitfield, A.T. Paschoalini, Towards an in-situ measurement of wave velocity in buried plastic water distribution pipes for the purposes of leak location. Journ. Soun. Vibr. 359 (2015) 40-55.
[4] F.C.L. Almeida, M.J. Brennan, F.K. de Lima, M.K. Iwanaga, O. Scussel, Using a geophone as an actuator to estimate the velocity of leak noise propagation in buried water pipes., Appl. Acouti. 184 (2021) 108251.
[5] F.C.L. Almeirda, M.J. Brennan, P.F. Joseph, Y. Gao, A.T. Paschoalini, The effects of resonances on time delay estimation for water leak detection in plastic pipes, Journ. Soun. Vibr. 420 (2018) 315-329.
[6] M.K. Iwanaga, M.J. Brennan, F.C.L. Almeida, O. Scussel, S.O. Cezar, A laboratory-based leak noise simulator for buried water pipes, Appl. Acoust. 185 (2022) 108346.
[7] M.J. Brennan, M. Karimi, J.M. Muggleton, F.C.L de Almeida, F. K. de Lima, P.C. Ayala, D. Obata, A.T. Paschoalini, N. Kessissoglou. On the effects of soil properties on leak noise propagation in plastic water distribution pipes, J. Sound Vib. 427 (2018) 120-133.
[8] Y. Gao, Y. Liu, J.M. Muggleton, Axisymmetric fluid-dominated wave in fluid-filled plastic pipes: Loading effects of surrounding elastic medium, Appl. Acoust. 116 (2017) 43-49.
[9] Q. Leclerè, A. Pereira, C. Bailly, J. Antoni, C. Picard, A unified formalism for acoustic imaging based on microphone array measurements, Int. Journ. Aeroacost. 16 (2017) 202-229.
[10] P. Chiariotti, M. Martarelli, P. Castellini, Acoustic beamforming for noise source localisation – Reviews, methodology and applications, Mech. Sys. And Sign. Proc. 120 (2019) 422-448.
[11] P.H.M.C Matos, E. Rustighi, V. Fontanari, and J. Muggleton. ”Preliminary Numerical Simulation for the Development of a Seismic Camera”. In Recent Trends in Wave Mechanics and Vibrations: Proceedings of WMVC 2022 (pp. 1085-1095). Cham: Springer International Publishing, 2022.
[12] A.N. Jette, J.G. Parker, Surface displacement accompanying the propagation of acoustic waves within an underground pipe, J. Sound Vib. 69 (2) (1980)

[13] Y. Gao, J.M. Muggleton,, Y. Liu, E. Rustighi. An analytical model of ground surface vibration due to axisymmetric wave motion in buried fluid-filled pipes. J. Sound Vib. 395 (2017) 142–159.
[14] J.M. Muggleton, M.J. Brennan, R.J. Pinnington,Wavenumber prediction in buried pipes for water leak detection, J. Sound Vib. 249 (5) (2002) 939-954.